Received: 25 March 2021 | Revised: 3 August 2021 | Accepted: 5 August 2021

DOI: 10.1002/cne.25230

RESEARCH ARTICLE

JCN RESEARCH IN SYSTEMS NEUROSCIENCE THE JOURNAL OF COMPARATIVE NEUROLOGY WILEY

Morphometric analysis of astrocytes in vocal production circuits of common marmoset (*Callithrix jacchus*)

Ariana Z. Turk | **Shahriar SheikhBahaei**

Neuron-Glia Signaling and Circuits Unit, National Institute of Neurological Disorders and Stroke, National Institutes of Health, Bethesda, Maryland, USA

Correspondence
Shahriar SheikhBahaei, Neuron-Glia Signaling and Circuits Unit, National Institute of Neurological Disorders and Stroke, National Institutes of Health, Bethesda, MD 20892, USA.
Email: sheikhbahaeis@nih.gov

Funding information
Intramural Research Program of the NIH, NINDS and NIMH, Grant/Award Number: ZIA NS009420-01

Abstract

Astrocytes, the star-shaped glial cells, are the most abundant non-neuronal cell population in the central nervous system. They play a key role in modulating activities of neural networks, including those involved in complex motor behaviors. Common marmosets (*Callithrix jacchus*), the most vocal non-human primate (NHP), have been used to study the physiology of vocalization and social vocal production. However, the neural circuitry involved in vocal production is not fully understood. In addition, even less is known about the involvement of astrocytes in this circuit. To understand the role, that astrocytes may play in the complex behavior of vocalization, the initial step may be to study their structural properties in the cortical and subcortical regions that are known to be involved in vocalization. Here, in the common marmoset, we identify all astrocytic subtypes seen in other primate's brains, including intralaminar astrocytes. In addition, we reveal detailed structural characteristics of astrocytes and perform morphometric analysis of astrocytes residing in the cortex and midbrain regions that are associated with vocal production. We found that cortical astrocytes in these regions illustrate a higher level of complexity when compared to those in the midbrain. We hypothesize that this complexity that is expressed in cortical astrocytes may reflect their functions to meet the metabolic/structural needs of these regions.

KEYWORDS
astrocytes, cerebral cortex, common marmoset, GFAP, glia, midbrain, vocalization

1 | INTRODUCTION

Astrocytes, the most numerous glial cells in the central nervous system (CNS), have historically been considered neuronal support cells primarily due to their role to maintain homeostasis in the CNS. Astrocytic homeostasis has come to include stabilization of ionic equilibrium (D'Ambrosio et al., 2002; Walz, 1989), metabolic control (Bröer et al., 1997; Dringen et al., 1993; Magistretti, 2006; Marina et al., 2018; Pellerin et al., 1998), clearance of neurotransmitter (Lehre et al., 1995; Wu et al., 2013) as well as maintenance of the blood–brain barrier and relationship with the neurovascular units (Haydon & Carmignoto, 2006; Mishra et al., 2016; Volterra & Meldolesi, 2005). While these functions are crucial for preserving a healthy brain, in recent years, it has become evident that astrocytes are not just "support cells" but actively communicate with neighboring neuronal cells. The astrocytic membrane contains receptors and transport mechanisms for neurotransmitters. In addition, they release gliotransmitters such as adenosine, ATP, glutamate, lactate, D-serine, prostaglandin E2, and others to modulate the activities of other brain cells (Anderson & Swanson, 2000; Araque et al., 2014; Bazargani & Attwell, 2016; Bezzi et al., 1998; Covelo & Araque, 2018; Durkee & Araque, 2019; Harada et al., 2015; Parpura & Haydon, 2000;

Sheikhbahaei, Turovsky, et al., 2018; Simard & Nedergaard, 2004). The capacity for astrocytes to take away and renew the neurotransmitters being released from neurons, as well as release of their own transmitter, portrays evidence that astrocytes may be modulating synaptic activity and contributing to neural networks' function. Therefore, it is proposed that astrocytes can play a key role in regulating complex behaviors and cognitive function (Halassa et al., 2009; Oberheim Bush & Nedergaard, 2017; Oliveira et al., 2015; Santello et al., 2019; Sheikhbahaei, Turovsky, et al., 2018).

Vocal production is a complex motor behavior that involves coordination of several brain regions and more than 100 muscles in the body. While the complete circuits are not fully elucidated, particular brain regions, including cerebral cortices, midbrain, and brainstem regions, have been illustrated as crucial for vocal production behaviors (Jarvis, 2019; Jürgens, 2002; Simonyan & Fuertinger, 2015). Recent data suggest that astrocytes are involved in regulation of complex motor circuits controlling locomotion (Christensen et al., 2013; Hegyi et al., 2009, 2018), mastication (Morquette et al., 2015), and respiration (Angelova et al., 2015; Rajani et al., 2018; Sheikhbahaei, Turovsky, et al., 2018). Therefore, it is plausible that astrocytes may also play a critical role in modulation of vocalization (Turk et al., 2021). In accordance with this hypothesis, it was suggested that a defect in astrocytes can lead to developmental stuttering (a common speech disorder that affects the fluency of speech) (Han et al., 2019; Maguire et al., 2021). Thus, it will be imperative to further understand the role of astrocytes in circuits that are involved in control of vocal production.

Previous work in rodents has identified morphological differences in astrocytic cellular structures that possibly reflect their physiological functions (Chai et al., 2017; Khakh & Sofroniew, 2015; Sheikhbahaei et al., 2018, b). Additionally, other glial cells, in particular microglia, have displayed morphological differences in specific CNS regions and illustrated that these differences are due to functional necessities (Berkiks et al., 2019; Doyle et al., 2017). While morphological analysis of astrocytes has previously been assessed in brainstem, midbrain, and some subcortical regions (Althammer et al., 2020; Chai et al., 2017; Mong & McCarthy, 2002; Reeves et al., 2011; Sheikhbahaei, Morris, et al., 2018; Tavares et al., 2017), only limited information is known about cellular architecture of cortical astrocytes (Eilam et al., 2016). Moreover, the majority of this work has been investigated in rodent models, with a few examples in human (Oberheim et al., 2006, 2009, 2012; Verkhratsky et al., 2018). Therefore, it is essential to fill the gap between rodent studies and human studies, possibly, by studying the morphometric characteristics of astrocytes in NHPs.

Common marmoset (*Callithrix jacchus)*, the most vocal NHP (Eliades & Miller, 2017; Miller et al., 2015), is relatively small (300–400 g, similar to size of a rat), but their brain structures and the ratio of gray matter to white matter are similar to those in human (Zilles et al., 1989). Therefore, marmosets might be a good model to investigate structural and functional properties of glia cells in regions involved the vocal production circuits. Accordingly, in this study, we used the adult common marmoset to perform a morphometric analysis of immunostained GFAP-positive astrocytes residing in cortical [rostral anterior cingulate cortex (ACC), ventral primary somatosensory cortex (SM1), primary auditory cortex (A1), ventral premotor cortex (A6Va), area 45 (A45)] and midbrain [central nucleus of the amygdala (CeA), ventral tegmental area (VTA), periaqueductal gray (PAG)] regions that are involve in vocalization. We identified all astrocyte subtypes that are described previously in primate and human brains (Oberheim et al., 2006, 2009, 2012; Verkhratsky et al., 2018). In addition, our data suggest that there are few structural differences among astrocytes in the cortical regions and among astrocytes in the midbrain regions. However, there was a substantial difference in astrocyte structure when comparing between cortical and midbrain regions. These structural differences reflect a possible difference in function for astrocytes in cortical and midbrain areas, such that greater complexity of cortical astrocytes could reflect a higher metabolic and/or structural demand that more nuanced astrocytes would be able to provide.

2 | METHODS

2.1 | Animals

Two adult common marmosets (*C. jacchus*) (1 male, 1 female, ages: 61 ± 3 months; weight: 402 ± 20 g) were used in this study. We complied with all relevant ethical regulations for animal testing and research. All procedures in this study were approved by the Animal Care and Use Committee of the Intramural Research Program of National Institute of Mental Health. Marmosets were housed in cages in pairs or alone in a room with a 12 h light/dark cycle. Their food and water intake were regulated, receiving food and water ad liberum.

2.2 | Tissue processing and immunohistochemistry

Adult marmosets were euthanized with an overdose of anesthesia sodium pentobarbital (100 mg/kg, i.p.) and transcardially perfused with 500 ml of phosphate-buffered saline (PBS, .1 M) solution followed by 4% paraformaldehyde (PFA) fixative. Subsequently, the brain was extracted and post-fixed for 3–5 days in the same PFA solution. The extracted brains were sent to NeuroScience Associates (NSA) to be sectioned at 50 μm. Floating slices were stored in antifreeze solution in −20°C until staining. Coronal sections were selected based on corresponding section in atlas (Paxinos et al., 2012).

Coronal sections were immunostained as described before (Sheikhbahaei, Morris, et al., 2018). Briefly, floating sections were quenched in PBS containing 10% methanol and 3% H_2O_2 to suppress background fluorescence. To perform antigen retrieval, 1% citrate buffer warmed to 80°C was used to unmask the proteins. The tissue was then incubated on a shaker for 48 h at 4°C with an antibody against glial fibrillary acidic protein (GFAP; Table 1). While one primary antibody was conjugated and did not require a secondary antibody,

TABLE 1 Primary antibody characterization

Antigen	Description of immunogen	Source, host species, catalog no. RRID	Dilution used
GFAP	GFAP isolated from cow spinal cord	DAKO, rabbit polyclonal, catalog #z-0334, RRID: AB_10013382	1:1000
GFAP	Purified glial filament protein	Sigma-Aldrich, mouse monoclonal Cy3 conjugate, MAB3402C3, RRID: AB_11213580	1:1000

other sections were incubated with a GFAP primary antibody that required secondary conjugation. Those sections were subsequently incubated in secondary antibodies conjugated to the fluorescent probes (1:500; donkey anti-rabbit Life Technologies, RRID: AB_2762834) for 1.5 h shaking at room temperature. A separate section before or after the one that used for GFAP staining was stained with Nissl. Briefly, the tissue was stained with NeuroTrace™ green fluorescent Nissl stain (1:200 in PBS, Life Technologies, catalog No. N-21480) for 20 min at room temperature. All sections were subsequently mounted onto microscope slides and covered in an anti-fading mounting medium. Using an inverted confocal laser scanning microscope (Zeiss LSM 510) with image acquisition settings with 1024 × 1024-pixel resolution, z-stack images of GFAP-positive astrocytes were obtained from the slice thickness at 20× and 40× within the cortical (ACC, SM1, A1, A6Va, and A45) and midbrain (CeA, VTA, and PAG) regions (see Figure 1 for representative sketch of regions). Nissl images were acquired using an AxioScan.Z1 slide scanner (Carl Zeiss, with a 20 × objective). To avoid possible experimental variation, immunostaining was conducted and processed by one investigator with the same solutions and imaging protocol.

2.3 | Antibody characterization

We used two different anti-GFAP antibodies to validate specificity of GFAP staining in the adult marmoset (see Figure 2a–c, and Table 1). Both of these GFAP antibodies have previously been successfully used to demonstrate astrocytes in human and NHPs (Dominy et al., 2019; Forny-Germano et al., 2014; Kang et al., 2018; Thiruvalluvan et al., 2016).

Isolated from cow spinal cord, the rabbit-polyclonal anti-GFAP antibody (1:1000; formerly DAKO, now Agilent, catalog #z-0334, RRID: AB_10013382) cross-reacts with an epitome of mouse, rat, and human cytoskeleton, the intra-cytoplasmic filamentous protein [manufacturer's technical information; (Eng, 1985; Eng et al., 2000)]. Additionally, this antibody stains a double band at 245-395kDA on Western Blot Analysis (Key et al., 1993).

The mouse monoclonal GFAP antibody (1:1000, Sigma-Aldrich, catalog #MAB3402C3, RRID: AB_11213580) reacts with human, pig, chicken, and rat GFAP (manufacturer's technical information). This GFAP antibody was raised against purified glial filament protein (Debus, Weber, & Osborn, 1983).

2.4 | Three-dimensional (3D) reconstruction of astrocytes

In sections with fully expressed GFAP-positive astrocytes, image z-stacks (Figure 3) were imported into Imaris software (Oxford Instruments, RRID: SCR_007370) where semi-automatic and automatic reconstructions of individual astrocytes were completed with the software's filament tracing tool (see Figure 4). All images were obtained from the center of the region of interest to minimize overlap from nearby regions. GFAP-positive astrocytes from six brain regions (ACC, SM1, A1, CeA, VTA, and PAG) were chosen for reconstruction (up to five astrocytes per image, one to five images per regions). Astrocytic processes were traced throughout the entire thickness of the sections by one investigator and verified by a second investigator. Using Imaris, the astrocytes were subsequently analyzed for structural quantification.

2.5 | Morphometric analysis of astrocytes

Fully traced astrocytes in Imaris were used to obtain morphometric data. Using the 3D filament data that were developed originally to analyze reconstructed neurons, we specifically ran morphometric analysis in the regions of interest. The features extracted included analysis to determine the unique astrocyte process morphology found in each region. This included sholl analysis (Sholl, 1953) and convex hull analysis (Costa, 1995). Since complexity of astrocytic processes increases with radial distance from the soma, sholl analysis quantifies astrocyte branches quantity, branch points, number of terminals as well as process length. This analysis utilized shell volumes between concentric spheres, each 1 μm apart, radiating out from the center of the soma (see Figure 2f). Importantly, the sholl analysis finds the number of intersections between processes and sphere at a given radius.

Because astrocytic processes branch from their primary processes to secondary and tertiary and then even further to fine leaflets and branchlets that are unrecognizable with GFAP staining, we used 3D convex hull analysis to assess the volume occupied by the astrocytic process. In convex hull analysis, the volume of astrocytes was estimated by enveloping the cell surface area, creating a polygon that joins terminal points of the processes as described before (Sheikhbahaei, Morris, et al., 2018) (see Figure 2e).

To normalize and properly compare the cell process complexity in disparate regions, we used a complexity index. While this calculation was originally developed to analyze neuronal dendrite, it has since been adapted to also evaluate astrocyte processes (Sheikhbahaei, Morris, et al., 2018). Complexity index was computed by using the following formula: (Σ terminal orders + number of terminals) × (total process length/number of primary branches), where the number of "terminal orders for each terminal point is calculated as the number of branches that appear in proceeding backward from the defined terminal to the cell soma" (Sheikhbahaei, Morris, et al., 2018).

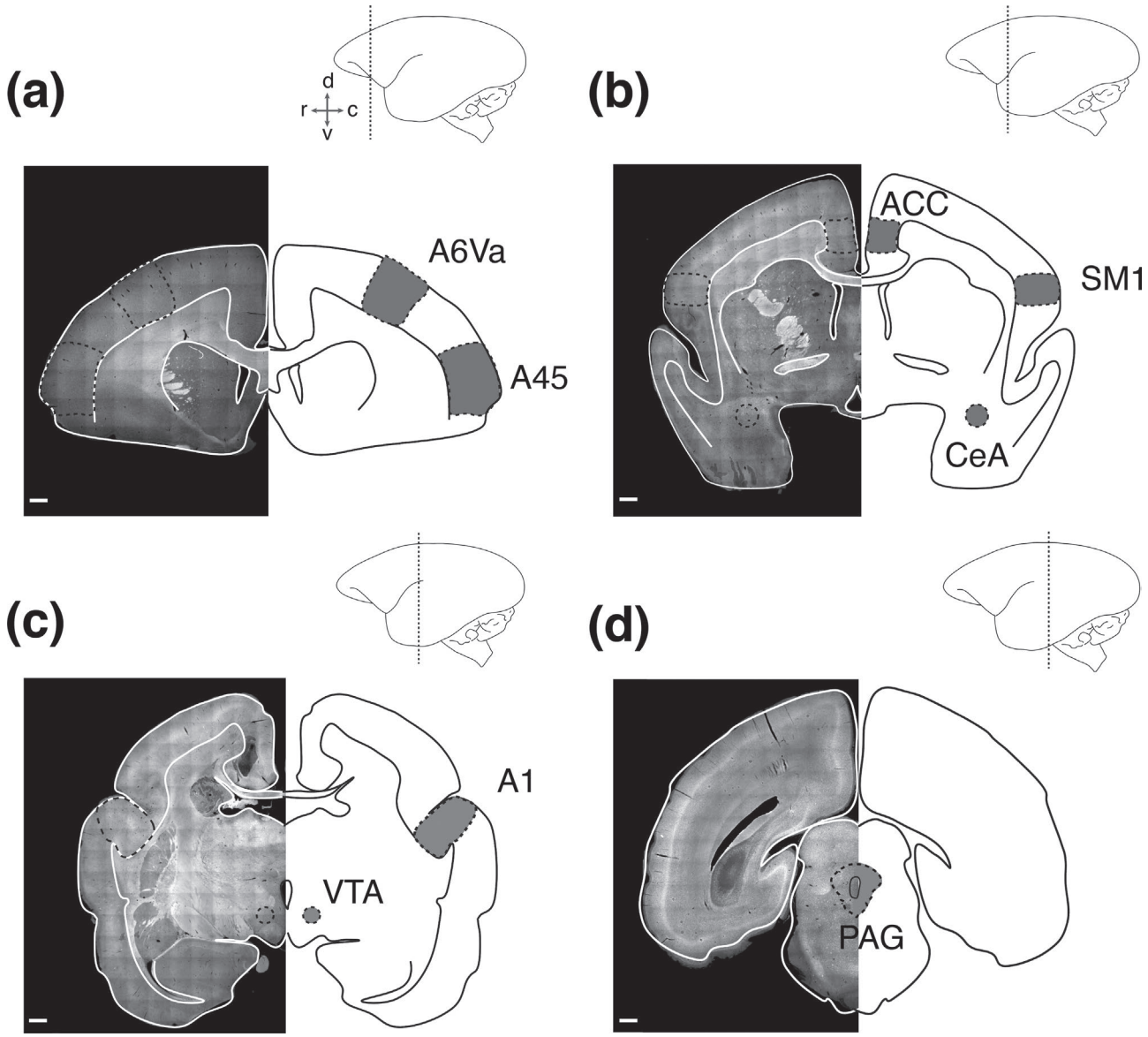

FIGURE 1 Schematic drawings of regions of interest in adult marmoset brain. (a) Locations of ventral premotor cortex (A6Va) and area 45 (A45) are shown on illustration (*right*) and Nissl-stained (*left*) coronal section. r—rostral, c—caudal, v—ventral, d—dorsal. (b) Illustration of a coronal section containing ventral primary sensorimotor cortex (SM1) corresponding to the orofacial region, rostral anterior cingulate cortex (ACC), and central nucleus of the amygdala (CeA) (*right*) is accompanied with Nissl staining from the corresponding section (*left*). (c) Location of primary auditory cortex (A1) and ventral tegmental area (VTA) in illustration (*right*) and Nissl-stained coronal slice (*left*). (d) Location of periaqueductal gray (PAG) is illustrated in coronal section from midbrain. Sagittal drawings of marmoset brain illustrate the regions of interest in each panel with a dashed line. Scale bars: 1 mm

2.6 | Statistical analyses

The analyzed data were exported from Imaris to Prism 9.0 software (Graphpad Software Inc., RRID: SCR_002798) where it was reported as averages ± standard error of mean (SEM). For statistical analysis, we used non-parametric Mann–Whitney *U* rank test or the Kruskal-Wallis one-way ANOVA by ranks followed by Dunn's post hoc test as appropriate. Evaluations with $p < .05$ were considered to be significant.

3 | RESULTS

3.1 | Distinction and categorization of marmoset astrocytes

We found primate-specific interlaminar astrocytes with cell bodies in layer I of the SM1 cortex and long, minimally branching processes terminating in the deeper cortical layers (Figure 5a). In addition, we observed fibrous astrocytes that have overlapping

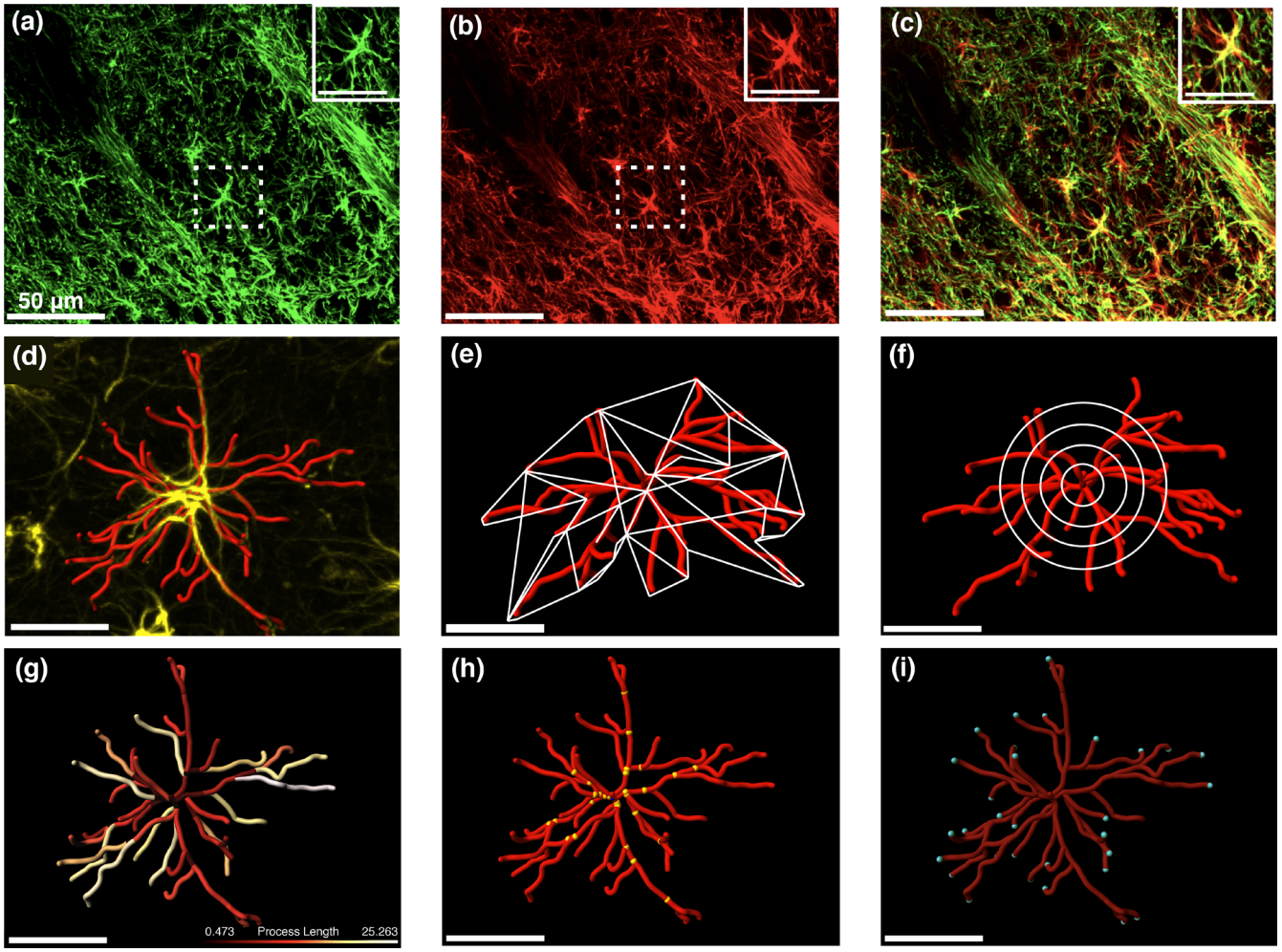

FIGURE 2 Antibody validation and methods to analyze morphometric characterization of astrocytes. (a–c) Ventrolateral brainstem immunostained GFAP-positive astrocytes with mouse anti-GFAP monoclonal antibody (green; a) and rabbit anti-GFAP polyclonal antibody (red; b). Merged low magnification and high magnification images. (c) Displays colocalization of both GFAP antibody labeling. (d) Semi-automated morphological 3D reconstructed astrocyte using Imaris in SM1. (e) Example of convex hull analysis in which the tips of each astrocytic process are connected to form a polygon in order to evaluate the space occupied by the astrocyte. (f) Portrayal of sholl analysis in which data points including branch points, terminal points, and process length are measured at each radial circle starting at the cell body and emanating outward. (g) Color-coated evaluation of process length where red indicates the shortest branches and white indicates the longest processes. (h and i) Display visualization of data from branch points (h) and terminal point (i), all data were generated using Imaris software [Color figure can be viewed at wileyonlinelibrary.com]

processes with neighboring astrocytes in the white-matter brain regions as well as corpus callosum (Figure 5b-c). Moreover, in cortical regions of the marmoset brain, we have identified gray matter protoplasmic astrocytes, which are described as spatially non-overlapping astrocytes (Figure 5d). In addition, primate-specific polarized astrocytes were present in marmoset cortical layers V and VI, close to blood vessels (Figure 5e). Lastly, we identified astrocytes that fit the description of varicose astrocytes, characterized by one to five long processes and multiple varicosities (Figure 5f). The interlaminar and polarized astrocytes were not very common among marmoset cortical astrocytes as we only detected them in SM1 and therefore were excluded from morphometric analysis.

3.2 | Morphometric characteristics of cortical astrocytes

The number of primary branches, number of branch points, number of terminal points, and process length were studied in ACC, A6Va, A45, SM1, and A1 astrocytes using the sholl analysis (see Figures 2 and 6 for more details). We found no differences in the average number of primary branches ($p > .9$, Kruskal-Wallis ANOVA by ranks followed by Dunn's post hoc test; Figure 7a). Similarly, when evaluating the number of branch points, we found no significant difference between astrocytes residing in these regions ($p > .9$, Kruskal-Wallis ANOVA by ranks followed by Dunn's post hoc test, Figure 7b). Likewise, when investigating the number of terminal points, we found no differences

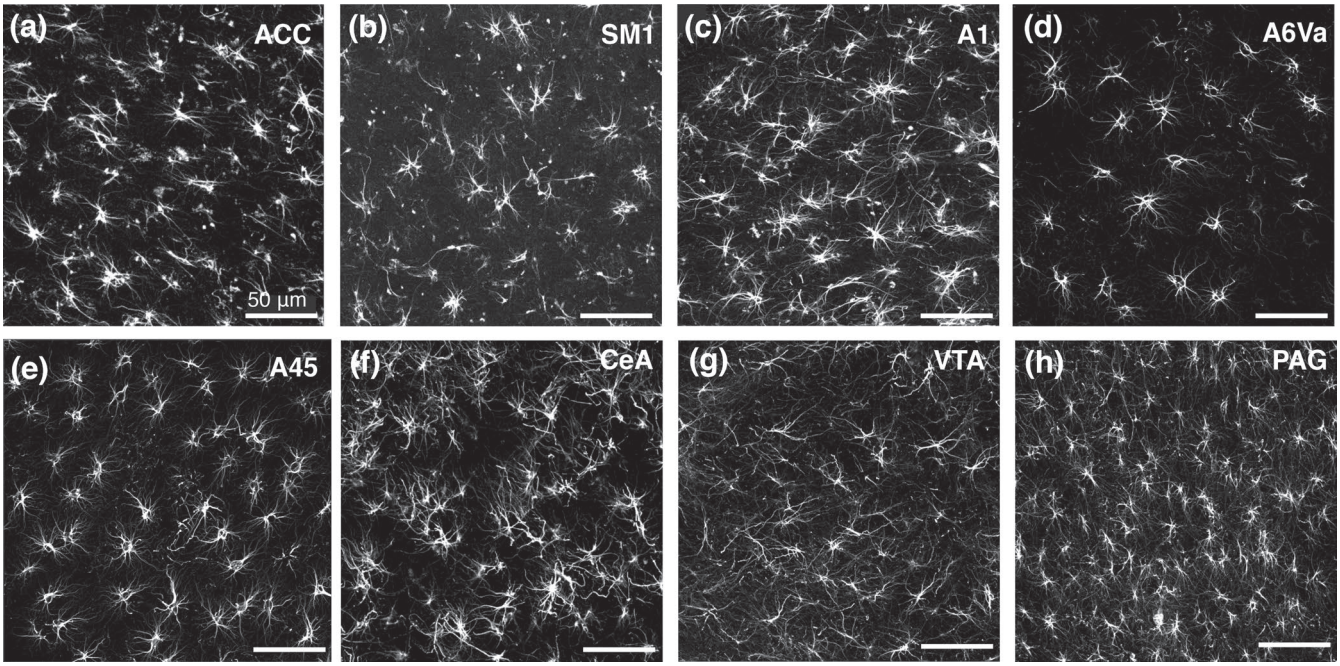

FIGURE 3 Immuno-stained GFAP-positive astrocytes in the adult marmoset cortex and midbrain. (a–e) Show the confocal images of cortical regions, including anterior cingulate cortex (ACC) (a), primary sensorimotor cortex (SM1) (b), primary auditory cortex (A1) (c), ventral premotor cortex (A6Va) (d), and area 45 (A45) (e). (f–h) Denote the confocal images of midbrain regions, including central nucleus of the amygdala (CeA) (f), ventral tegmental area (VTA) (g), and periaqueductal gray (PAG) (h)

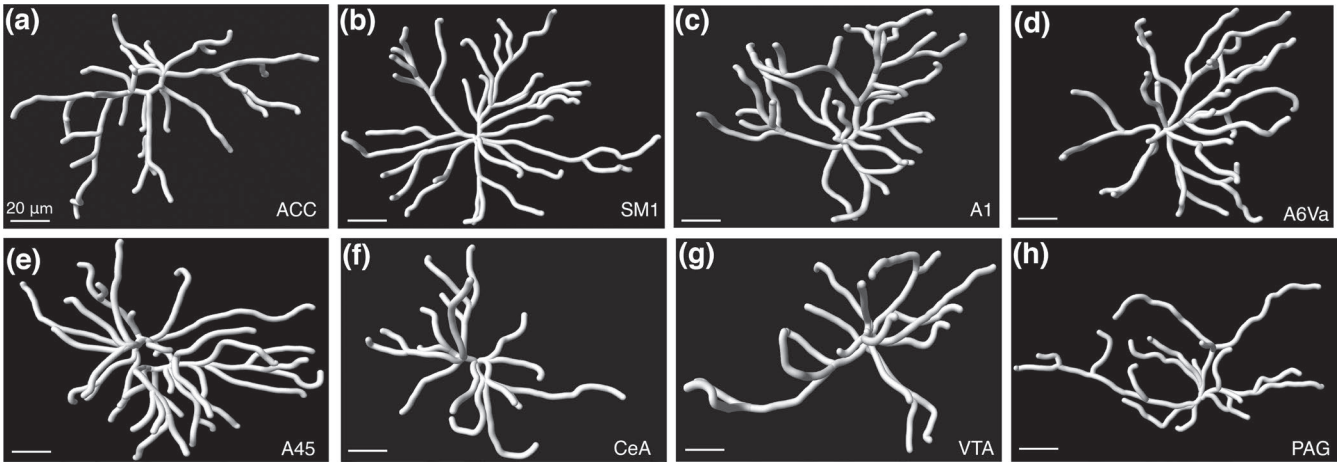

FIGURE 4 Example reconstructed GFAP-positive astrocytes in the adult marmoset cortex and midbrain. (a–e) Example of reconstructed cortical astrocytes in (a) anterior cingulate cortex (ACC), (b) primary sensorimotor cortex (SM1), (c) primary auditory cortex (A1), (d) ventral premotor cortex (A6Va), and (e) area 45 (A45). (f–h) Illustrate reconstructed midbrain astrocytes residing in (f) central nucleus of the amygdala (CeA), (g) ventral tegmental area (VTA), and (h) periaqueductal gray (PAG)

between ACC, A6Va, A45, SM1, and A1 astrocytes ($p > .9$, Kruskal-Wallis ANOVA by ranks followed by Dunn's post hoc test; Figure 7c).

On the other hand, the averaged process length of SM1 astrocytes was significantly larger than ACC, A6Va, A45, and astrocyte processes ($p = .016$, $p < .001$, $p < .001$, and $p = .029$, respectively; Mann–Whitney *U* rank test). However, no differences were observed in astrocytic process lengths between ACC, A6Va, A45, and A1 regions ($p = .9$, Mann–Whitney *U* rank test, Figure 7d). Surface area of SM1 astrocytes proved to be larger than astrocytes in ACC ($p < .001$, Mann–Whitney *U* rank test) as well as astrocytes residing in A6Va, A45, and A1 ($p = .001$, $p < .001$, and $p = .005$, Mann–Whitney *U* rank test). However, no differences in surface area were found between astrocytes in ACC, A6Va, A45, and A1 ($p = .9$, Kruskal-Wallis ANOVA by ranks followed by Dunn's post hoc test; Figure 8a). While the convex hull analysis found differences in surface area, no such difference was found when evaluating the convex hull volume of ACC, SM1, and A1 astrocytes ($p > .9$, Kruskal-Wallis ANOVA by ranks followed by Dunn's post hoc test; Figure 8b). We also evaluated

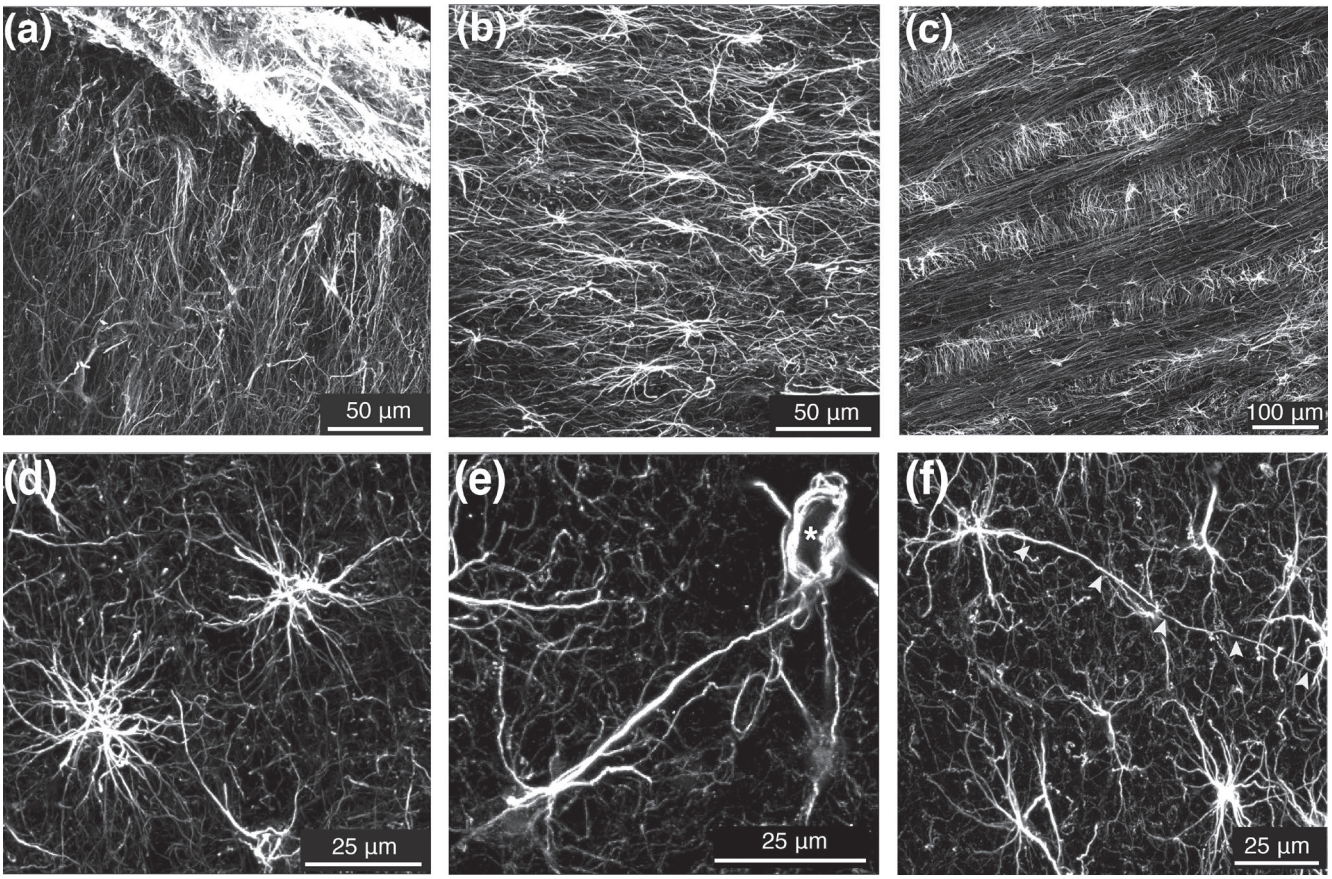

FIGURE 5 Astrocyte subtypes observed in the marmoset brain. All five astrocyte subtypes that were previously described human and other primate species were observed in marmoset brain. (a) Interlaminar astrocytes in layers I and II of the primary sensorimotor cortex (SM1) cortex (b and c) fibrous astrocytes displayed in the white matter tissue with overlapping and intermingling processes. (b) Astrocytes found in the ventral tegmental area (VTA) and (c) astrocytes seen in the anterior commissure. (d) Spatially distinct protoplasmic astrocytes found in layers VI-V of the SM1 cortex. (e) Example of polarized astrocyte in layer V of SM1 in close proximity and interacting with a blood vessel (marked by *). (f) Illustrates a varicose astrocyte in layer V of SM1 with one long process (marked with white arrowheads) extended and multiple varicosities observed along the process

astrocytes via a complexity index (see Methods for more details) to compare the overall complexity of astrocytes' morphology in various regions. While differences were observed in many of the individual measures, the overall complexity indices of astrocytes in ACC compared to those in SM1 and A1 were not different ($p = .3$, $p > .9$, respectively; Mann–Whitney *U* rank test) and the complexity index comparison between SM1 and A1 astrocytes also showed no differences ($p = .9$, Mann–Whitney *U* rank test). However, differences in complexity indices were only observed between A6Va and SM1 as well as between A45 and SM1 astrocytes ($p = .01$, $p = .002$, respectively, Mann–Whitney *U* rank test; Figure 9).

3.3 | Morphological features of midbrain and brainstem astrocytes

We then evaluated morphometric features of the astrocytes from CeA, VTA, and PAG, regions that have shown to be also involved in vocal production. We first compared the number of primary branches per astrocyte in each region and found no differences between the measurements from these three midbrain regions ($p > .9$, Kruskal-Wallis ANOVA by ranks followed by Dunn's post hoc test; Figure 7a). We then analyzed the number of branch points from astrocytes residing in these three regions and similarly found not difference ($p = .9$, Mann–Whitney *U* rank test; Figure 7b). Although, the number of terminal points of VTA astrocytes was greater than CeA astrocytes ($p = .003$, Mann–Whitney *U* rank test), the number of terminal points measured from PAG astrocytes was similar to astrocytes found in VTA and CeA ($p = .4$, .1, respectively, Mann–Whitney *U* rank test; Figure 7c).

We then evaluated and compared process length of the midbrain astrocytes. Our findings indicate that VTA astrocyte length, on average, was larger than CeA astrocytes ($p = .007$, Mann–Whitney *U* rank test) but not PAG astrocytes ($p = .3$, Mann–Whitney *U* rank test). CeA and PAG astrocytes were also found to show no differences in process length ($p = .1$, Mann–Whitney *U* rank test; Figure 7d).

Subsequently, we acquired and analyzed the convex hull surface area and volume of the midbrain astrocytes. Our findings indicate no significant region to region variation in surface area ($p > .9$, Kruskal-Wallis ANOVA by ranks followed by Dunn's post

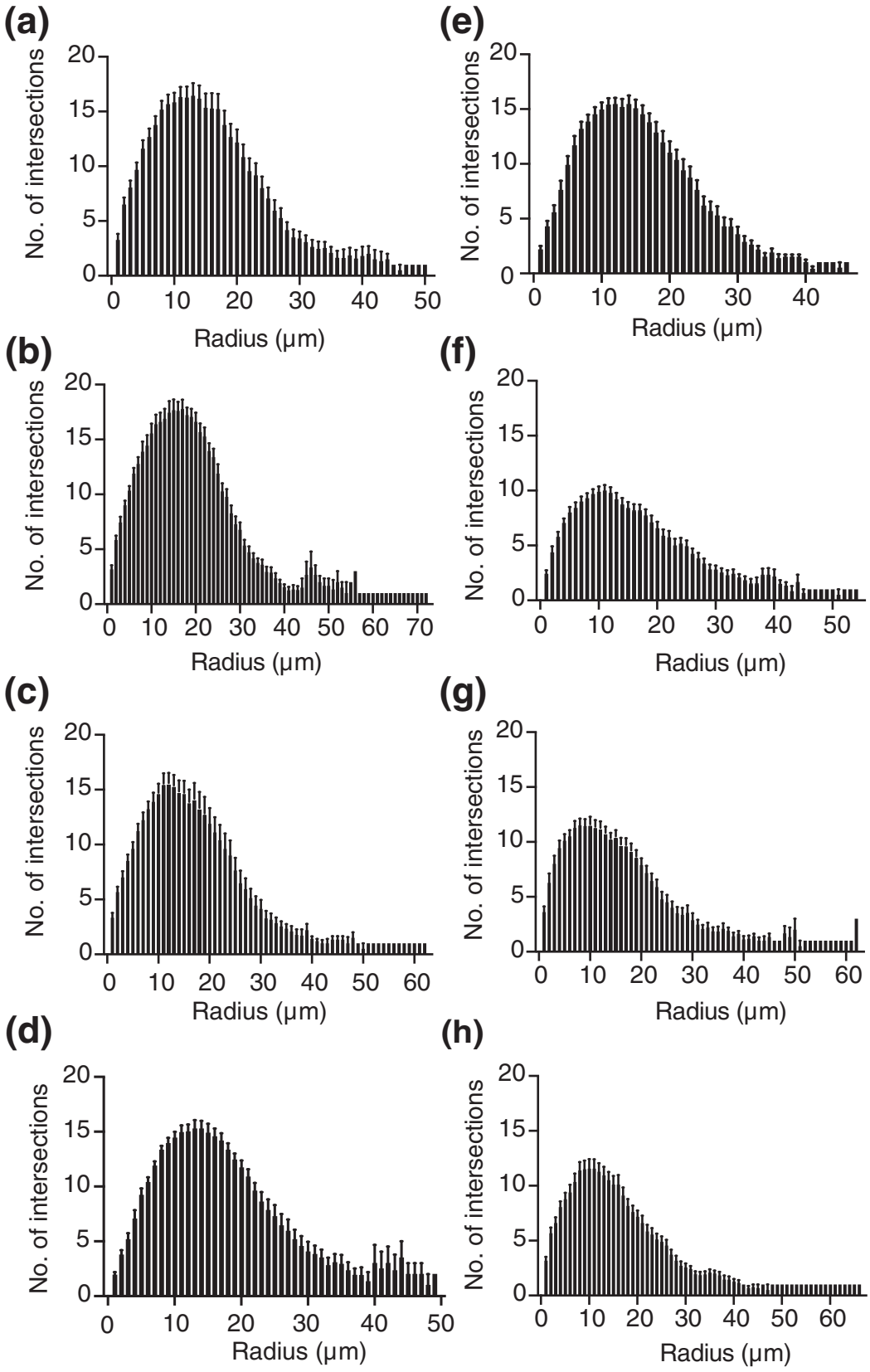

FIGURE 6 Summary of region-by-region sholl analyses. Averaged process intersections at each spherical point emanating from the astrocyte cell body is displayed. Left column and first graph in the right column (a–e) displays cortical regions, anterior cingulate cortex (ACC) (a), primary sensorimotor cortex (SM1) (b), primary auditory cortex (A1) (c), ventral premotor cortex (A6Va) (d), area 45 (A45) (e) and the rest of the right column (f–h) illustrates midbrain regions, central nucleus of the amygdala (CeA) (f), ventral tegmental area (VTA) (g), periaqueductal gray (PAG) (h)

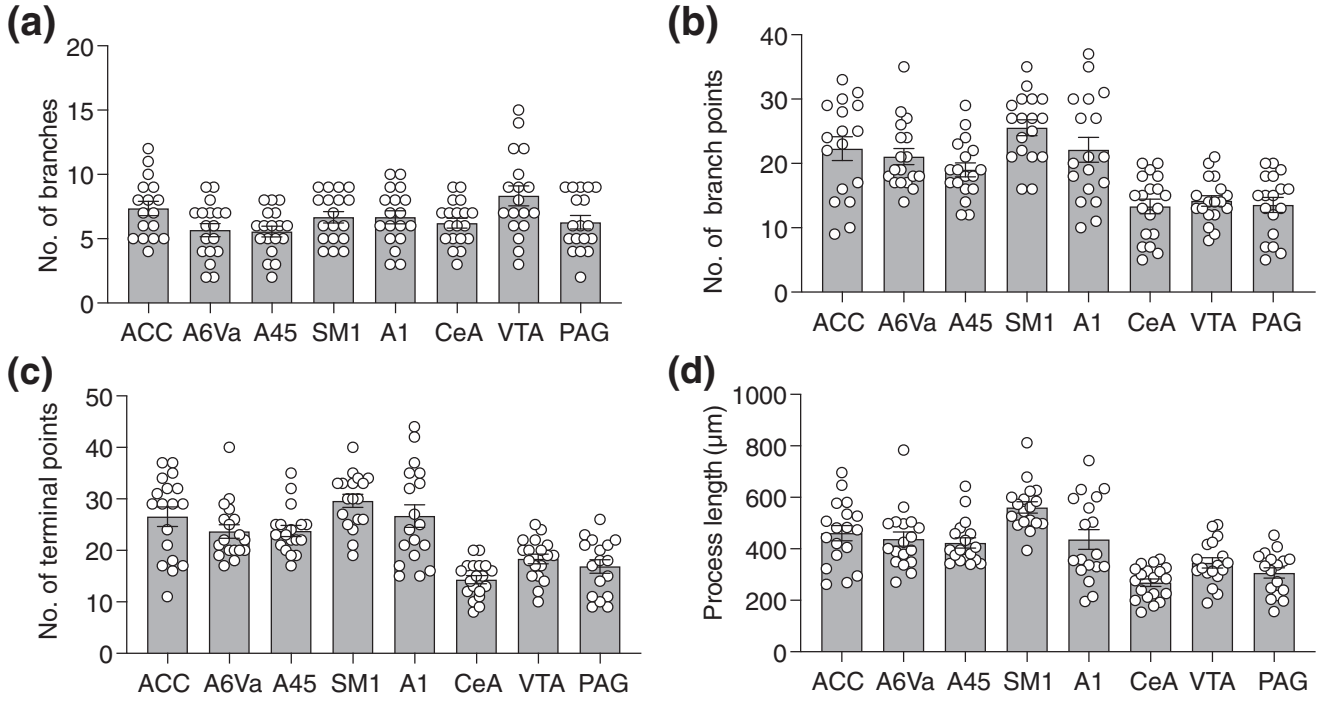

FIGURE 7 Morphometric features of cortical and midbrain astrocytes. Group morphological data obtained using sholl analysis: (a) number of primary branches, (b) number of branch points, (c) number of terminal points, and (d) process length of anterior cingulate cortex (ACC) ($n = 18$), ventral premotor cortex (A6Va) ($n = 18$), area 45 (A45) ($n = 18$), primary sensorimotor cortex (SM1) ($n = 18$), primary auditory cortex (A1) ($n = 18$), central nucleus of the amygdala (CeA) ($n = 19$), ventral tegmental area (VTA) ($n = 18$), and periaqueductal gray (PAG) ($n = 18$) (see Table 2 for more details). On average, cortical astrocytes have longer processes, more branch points, and terminal points. All statistical differences are indicated in results section and Table S1

hoc test; Figure 8a). While no differences were seen in area, the volume of astrocytes in VTA proved to be significantly larger than both the volume of CeA astrocytes ($p = .007$, Mann–Whitney *U* rank test) and PAG astrocytes ($p = .004$, Mann–Whitney *U* rank test; Figure 8b). A complexity index was used to evaluate over all morphometric characteristics of astrocytes residing in CeA, VTA, and PAG. Our findings indicate no differences in complexity between any of the midbrain and brainstem regions ($p > .9$, Kruskal-Wallis ANOVA by ranks followed by Dunn's post hoc test; Figure 9).

In addition, since anterior striatum is involved in vocal production, we also attempted to evaluate striatal astrocytes. However, no GFAP-positive astrocytes were observed in the striatum of marmoset; these results are similar to previously reported data in NHP tissue within the striatum (De Salles et al., 2001; Himeda et al., 2006).

3.4 | Comparison of morphological features of cortical and midbrain astrocytes

We also compared the number of primary branches, branch points, and number of terminal points of astrocytes in the cortical regions (ACC, A6Va, A45, SM1, A1) with those of astrocytes in the midbrain regions (CeA, VTA, PAG). Our data suggest that astrocytes in cortical regions, overall, have a greater number of branch points and terminal points when compared to midbrain astrocyte data (Kruskal-Wallis ANOVA by ranks followed by Dunn's post hoc test; Tables 2 and S1). However, no significant differences were observed in number of primary branches (Kruskal-Wallis ANOVA by ranks followed by Dunn's post hoc test; Tables 2 and S1). Additionally, a comparison of astrocyte process length between cortical and midbrain regions indicated that cortical astrocytes are generally longer than midbrain astrocytes (Kruskal-Wallis ANOVA by ranks followed by Dunn's post hoc test; Figure 7; Tables 2 and S1).

Convex hull assessment of volume and surface area was also compared between astrocytes in the cortex and midbrain. While cortical astrocytes displayed greater volume compared to midbrain astrocytes ($p < .001$, Kruskal-Wallis ANOVA by ranks followed by Dunn's post hoc test), this finding was not observed in surface area where only astrocytes from SM1 proved to be larger than midbrain astrocytes ($p < .001$, Kruskal-Wallis ANOVA by ranks followed by Dunn's post hoc test; Figure 8). While no differences were observed in astrocyte complexity within cortical or midbrain regions, significant differences were displayed between cortical and midbrain astrocytes. Our data suggested that cortical astrocytes, on average, are more complex when compared to midbrain astrocytes (Figure 9, Tables 2 and S1).

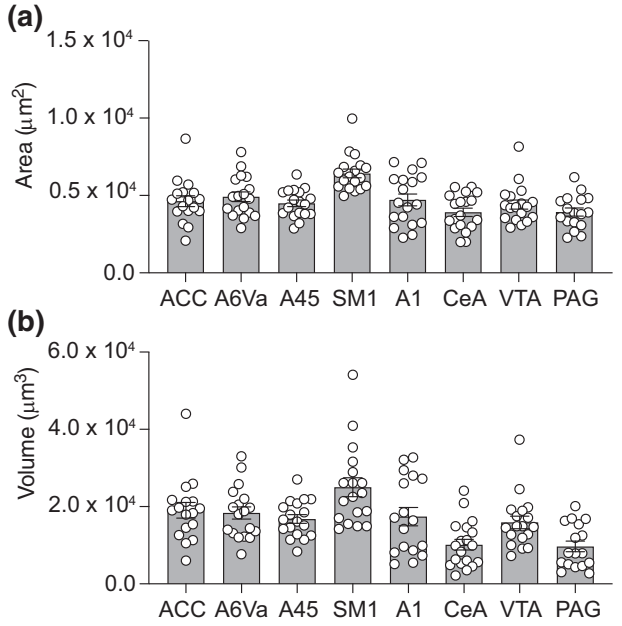

FIGURE 8 Convex hull analysis of cortical and midbrain astrocytes. Summary of data from convex hull volume (a) and surface area (b) analyses in anterior cingulate cortex (ACC) ($n = 18$), ventral premotor cortex (A6Va) ($n = 18$), area 45 (A45) ($n = 18$), primary sensorimotor cortex (SM1) ($n = 18$), primary auditory cortex (A1) ($n = 18$), central nucleus of the amygdala (CeA) ($n = 19$), ventral tegmental area (VTA) ($n = 18$), and periaqueductal gray (PAG) ($n = 18$). On average, SM1 astrocytes have a larger volume and surface area compared to the astrocytes in the other regions evaluated

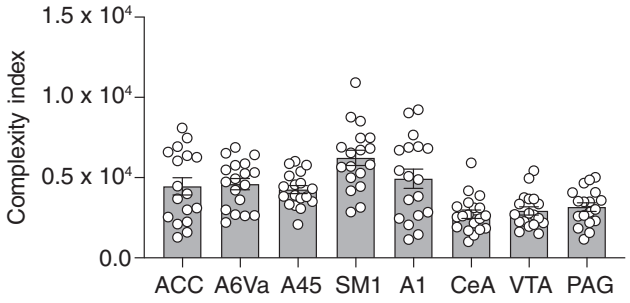

FIGURE 9 Complexity indices of astrocytes in cortical and midbrain regions. Comparison of data in each region measuring the morphological complexity of astrocytes. This measurement was obtained using a complexity index (see Methods) applied to the semi-automatic reconstructed astrocytes in the regions of interest. Overall, cortical astrocytes were more complex compared to midbrain astrocytes

4 | DISCUSSION

In this study, we investigated the structural properties of astrocyte morphology within the vocalization circuits of adult common marmosets. While the brain circuits that control vocal production are not fully understood, it is accepted that certain cortical and midbrain regions are involved in the execution of this complex behavior (Jarvis, 2019; Jürgens, 2002). While vocalization could be an innate behavior involving midbrain regions (including CeA, VTA, and PAG), voluntary vocalization is considered a cognitive function and therefore, involves a variety of cortical regions. These cortical regions include sensory (such as SM1 and A1) as well as frontal regions (including ACC, area 6Va, and A45). Area 45 has been defined as a homolog of human's Broca's area and as such, may be important for vocalization (Bakola et al., 2015; Burman et al., 2015; Petrides et al., 2005; Simões et al., 2010; Theodoni et al., 2020). Since it is plausible that, similar to other complex motor circuits, astrocytes may also modulate the vocal motor circuits, we investigated the morphometric properties of astrocytes from both cortical and midbrain regions that have been previously suggested to be involved in vocal production circuits.

4.1 | Astrocytes

Astrocytes are the star-shaped glial cells with several long processes stemming from the soma. The primary branches split into numerous secondary and tertiary branches with fine branchlets and leaflets holding the space in between the thicker processes. These complex glial cells are found throughout all regions of the CNS in communication with other glia cells, neurons and the vascular system. Astrocytes play myriad roles throughout the CNS, including maintaining ionic and metabolic balance as well as clearance and reuptake of neurotransmitters (D'Ambrosio et al., 2002; Lehre et al., 1995; Magistretti, 2006; Wu et al., 2013). While these functions are necessary to keep the brain healthy and running smoothly, it has become evident that astrocytes also play an active role in regulation of brain circuits controlling complex behaviors.

Here, we used immunostaining against GFAP to extract the cellular architecture of astrocytes in six distinct brain regions (Figure 1, Figure 3), each of which are involved in vocal production behaviors in common marmoset. GFAP, a protein specifically expressed in mature astrocytes of the CNS, was used to delineate astrocytic complexity in the regions of interest (see Sheikhbahaei, Morris, et al., 2018 for details regarding GFAP staining). However, GFAP immunostaining might underestimate the complexity of astrocyte's processes and is not expressed by all astrocytes (Yu et al., 2020). In addition, in the rodent hippocampus, it has been estimated ~15% of total astrocyte volume contained GFAP-positive filaments. This is because fine astrocytic processes, such as small branchlets and leaflets, are GFAP-negative (Bushong et al., 2002). However, there is also evidence that when hippocampal astrocytes are filled with lipophilic dyes (which reveals the finest processes) and compared to GFAP immuno-labeled astrocytes (which does not delineate the finest processes), there were no significant differences between measured values of astrocyte diameter, as well as process length and thickness (Oberheim et al., 2008). Additionally, it has been shown that in the rat brainstem, that thickness and main process length of astrocytes that are virally transduced to express green fluorescent protein (GFP) were similar to

TABLE 2 Individual values (mean ± *SEM*) of all analyzed parameters for astrocyte morphology

	ACC $n = 18$	SM1 $n = 18$	A6Va $n = 18$	A45 $n = 18$	A1 $n = 18$	CeA $n = 19$	VTA $n = 18$	PAG $n = 18$
Total number of branches	7 ± .5	7 ± .4	6 ± .5	6 ± .4	7 ± .5	6 ± .4	8 ± .8	6 ± .5
Number of branch points	22 ± 2	25 ± 2	21 ± 1	19 ± 1	22 ± 2	13 ± 1	14 ± 1	13 ± 1
Number of terminal points	27 ± 2	30 ± 1	24 ± 1	24 ± 1	27 ± 2	14 ± 1	18 ± 1	17 ± 1
Process length (µm)	450 ± 33	561 ± 22	434 ± 28	423 ± 20	436 ± 38	268 ± 15	345 ± 20	305 ± 19
Surface area (μm^2)	4628 ± 280	6424 ± 349	4919 ± 309	4488 ± 212	4714 ± 383	3915 ± 266	4411 ± 293	3716 ± 28
Volume (μm^3)	19,053 ± 2015	25,017 ± 2456	18,355 ± 1594	16,794 ± 1121	17,401 ± 2397	10,144 ± 1377	15,905 ± 1630	9140 ± 1402
Complexity index	4456 ± 651	7232 ± 917	4595 ± 351	4256 ± 253	4927 ± 602	2716 ± 261	2926 ± 254	3164 ± 265

Note: *n*, number of astrocytes analyzed per region.

those immunostained against GFAP (Sheikhbahaei, Morris, et al., 2018). Although GFAP immunostaining has limitations, this method is still very reliable for the analysis of key morphometric characteristics of astrocytes, including branch processes, allowing for comparative analyses, which was the main focus of this study.

Other astrocytic markers (s100ß, Aldh1, Sox9, GLT1, GLAST) are also able to illustrate some astrocyte details; however, they hold their own limitations (see Sheikhbahaei, Morris, et al., 2018 and Yu et al., 2020 for more details). Additionally, other techniques have been introduced to gain insight into specific details of astrocyte morphology. For example, intracellular dye-filling allows for detailed investigation of fine astrocytic processes at the single-cell level. While the intricate details of the fine astrocyte processes can be examined, this method is time-consuming and only allows for an evaluation of a small number of astrocytes (Moye et al., 2019; Zhou et al., 2019). Electron microscopy is another method being used to comprehend the morphometric features of astrocytes as it allows for a 3D reconstruction of serial sections. This method includes a tissue fixation technique that might affect the preservation of astrocytic structure (Korogod et al., 2015; Ventura & Harris, 1999).

To analyze the morphometric processes of the astrocytes, computer-aided morphometric analyses were used to investigate the structural features of CNS astrocytes potentially contributing to their functional role. Imaris software (or other software such as Neurolucida 360) has been previously used to study the morphology of astrocytes and other glial cells (Althammer et al., 2020; Cengiz et al., 2019; Hefendehl et al., 2014; Radford et al., 2015; Sheikhbahaei, Morris, et al., 2018; Smith & Bilbo, 2019; Wagner et al., 2013). While other methods have been developed for the purpose of analysis of cellular morphology (Heindl et al., 2018; Karperien et al., 2013; Xu et al., 2016), these approaches are time-consuming and may result in an over- or under-sampling of the cells given that overlapping or cut-off cells are included in the analysis. Computer-aided analysis holds advantages as it allows for a quick, unbiased, automated reconstruction (Althammer et al., 2020). Additionally, the user-friendly interface of Imaris easily allowed us to integrate immunostained cells and reconstructed images into one interface to smoothly extract data for analysis.

There are five distinct subtypes of astrocytes that have been characterized in various species: (1) protoplasmic astrocytes, (2) polarized astrocytes, (3) fibrous astrocytes, (4) interlaminar astrocytes, and (5) varicose astrocytes (Oberheim et al., 2006, 2009). It has been suggested that the rodent brain only features protoplasmic and fibrous astrocytes (Oberheim et al., 2006). Whereas the primate brain also contains polarized and interlaminar astrocytes (Oberheim et al., 2006) and varicose astrocytes have only been observed in higher-order primate (Oberheim et al., 2009). Our data suggest that all astrocyte subtypes exist in marmoset brain, including varicose astrocytes that were only previously observed in higher-order primates (Oberheim et al., 2009), (Figure 5f). Traditionally, interlaminar astrocytes described as dense and numerous in the Old world primate, ape, and human brain, and devoid from the New World monkey brain, in particular the marmoset brain (Colombo, 1996, 2017, 2018; Colombo

et al., 2000; Colombo & Reisin, 2004). However, this view was challenged recently, as interlaminar astrocytes were found in many mammals including common marmoset (Falcone et al., 2019). Here, we found interlaminar astrocytes residing in layer I of the marmoset primary somatosensory cortex. While these astrocytes were not as dense as those described in other primate brains, our data further confirm the existence of interlaminar astrocytes in marmoset brain (Figure 5a). Since we did not observe interlaminar astrocytes in A1, 6Va, and A45 regions, though further studies are required, it is possible that interlaminar astrocytes are specific to some cortical regions (including SM1 region) in common marmoset.

4.2 | Marmosets

On an anatomical level, the orofacial movements and rhythmic movements observed in primates are similar to the oscillatory patterns humans use when vocalizing (Ghazanfar et al., 2012; Morrill et al., 2012). While these facial patterns are seen across primates, unlike Old World monkeys (such as rhesus macaques), common marmosets have the ability to create flexible vocalizations in research setting (Ghazanfar et al., 2019). The common marmoset is a widely used animal model for neuroscientific research as they hold advantages in being small primates (Power et al., 2001). Additionally, marmosets live in highly social environments and, importantly, have rich vocal communications (Miller et al., 2016; Okano et al., 2012; Pomberger et al., 2019). Marmoset vocal production is not just an autonomic response but their vocal repertoire ranges acoustically and includes responses to their social environment and to conspecifics (Bergman et al., 2019; Eliades & Miller, 2017; Ghazanfar et al., 2019). They can control what, where, and when to vocalize (Bergman et al., 2019). These communicative behaviors, at least on a rudimentary level, are similar to the mechanisms used in humans and therefore it is hypothesized that human speech is evolutionarily adapted from primates (Eliades & Miller, 2017). While marmosets have been used to study the physiology of vocalization (Gustison et al., 2019; Miller et al., 2015) and social vocal production (Kato et al., 2014; Sadagopan et al., 2015), little is known about the neuronal circuitry involved in vocal production and even less is known about the involvement of astrocytes within the vocalization circuits.

While the morphology and functions of astrocytes are mainly studied in rodents, human astrocytes are ~2.5-fold larger and more complex compared to rodents' astrocytes (López-Hidalgo & Schummers, 2014; Oberheim et al., 2006, 2009). Since the function of brain cells is intimately related to the cell's morphology, it is plausible that the function of astrocytes should be more elaborate in humans compared to rodents. In this setting, using the common marmoset as a primate animal model to study astrocyte morphology and function might be advantageous. Their brain similarities to other primates (such as analogous brain regions, similar gray-to-white matter ratio) and rodents (similar brain size) make marmoset an attractive animal model to fill the research gap between humans and rodents.

4.3 | Cortical versus midbrain astrocytes

While our data suggest that no significant differences were observed between morphology of astrocytes residing in the cortical or in the midbrain regions, profound differences were displayed between cortical and midbrain astrocytes. These differences extend to include astrocytic process complexity, volume, and surface area. These morphometric differences observed are in line with other findings in rodents that illustrate regional differences in the morphology and function of astrocytes. For instance, it has been shown that while ventral brainstem astrocytes respond to changes in pH by releasing ATP, cortical astrocytes have no such pH sensitivity and response (Kasymov et al., 2013). In addition, a variance in astrocytic regulation of excitatory synapses as well as a differential gene expression profile for synaptogenic factors in cortical and midbrain astrocytes are reported (Buosi et al., 2018). Moreover, it has been shown that astrocytes in the midbrain are physiologically distinct from those in the cortex such that midbrain astrocytes have a lower membrane resistance, are extensively coupled to oligodendrocytes through gap junctions, and have intracellular calcium activity that is particularly modulated by dopamine 2 receptor signaling (Xin et al., 2019). Other data suggest that the epidermal growth factor receptor (EGFR) signaling seemed to be regulated by astrocytes within the mouse cortex whereas midbrain astrocytes do not such a role (Wagner et al., 2006). Therefore, since cortical and midbrain astrocytes are functionally distinct, it is plausible that their morphology should be different as well. Additionally, we acknowledge that other cortical and subcortical regions may play a role in vocal production behaviors (Burman et al., 2008). Therefore, future experiments are required to investigate cellular properties of astrocytes (and other distinct cell types) residing in those regions that may further elucidate circuit-dependent astrocytic properties at the cellular and functional levels.

4.4 | Concluding remarks

Astrocytes are remarkably integrated into neural networks in both the cortex and midbrain where they may be involved in regulation of complex motor behaviors, including the vocalization. Here, our data suggest that the overall cellular architecture of cortical astrocytes is more complex than astrocyte in midbrain regions. Although we cannot rule out the possible constraints imposed by structural features of associated neurons (including pyramidal neurons in the cortical areas) or the parenchymal characteristics of the brain regions, we hypothesize that the differences in astrocyte morphology illustrated here could be related to their distinct functions. Higher order brain regions may require more complex metabolic and structural support than midbrain regions because of the cognitive function they play. Thus, cortical regions may demand astrocytes to maintain a more dynamic, complex structure and function. Our data also provide a framework for future morphometric analysis of astrocytes in the primate brain. For instance, since vocalization is known to be lateralized to the left hemisphere

(Fuertinger et al., 2018; Vigneau et al., 2006), it may be important to further investigate if there is a lateralized morphological differences in astrocytes. Understanding more about the role of astrocytes in control of complex motor behaviors might provide additional information for cell-targeting for novel pharmacogenomic strategies to interfere with motor control disorders, such as speech fluency disorders.

ACKNOWLEDGMENTS

The authors thank NINDS Light Microscopy Core and NIMH Systems Neuroscience Imaging Resource (SNIR) for technical assistances. The authors also thank Mitchell Bishop for technical assistance. The authors are grateful to Dr. David Leopold for supports and comments on an earlier version of the manuscript. This work was supported by the Intramural Research Program of the NIH, NINDS, and NIMH (ZIA NS009420-01).

CONFLICT OF INTEREST

The authors declare no competing financial interests.

PEER REVIEW

The peer review history for this article is available at https://publons.com/publon/10.1002/cne.25230.

DATA AVAILABILITY STATEMENT

Data availability The data that support the findings of this study are available from the corresponding author upon reasonable request.

ORCID

Shahriar SheikhBahaei https://orcid.org/0000-0003-4119-9979

REFERENCES

Althammer, F., Ferreira-Neto, H. C., Rubaharan, M., Roy, R. K., Patel, A. A., Murphy, A., Cox, D. N., & Stern, J. E. (2020). Three-dimensional morphometric analysis reveals time-dependent structural changes in microglia and astrocytes in the central amygdala and hypothalamic paraventricular nucleus of heart failure rats. *Journal of Neuroinflammation*, *17*, 221.

Anderson, C. M., & Swanson, R. A. (2000). Astrocyte glutamate transport: Review of properties, regulation, and physiological functions. *Glia*, *32*, 1–14.

Angelova, P. R., Kasymov, V., Christie, I., Sheikhbahaei, S., Turovsky, E., Marina, N., Korsak, A., Zwicker, J., Teschemacher, A. G., Ackland, G. L., Funk, G. D., Kasparov, S., Abramov, A. Y., & Gourine, A. V. (2015). Functional oxygen sensitivity of astrocytes. *The Journal of Neuroscience*, *35*, 10460–10473.

Araque, A., Carmignoto, G., Haydon, P. G., Oliet, S. H. R., Robitaille, R., & Volterra, A. (2014). Gliotransmitters travel in time and space. *Neuron*, *81*, 728–739.

Bakola, S., Burman, K. J., & Rosa, M. G. P. (2015). The cortical motor system of the marmoset monkey (*Callithrix jacchus*). *Neuroscience Research*, *93*, 72–81.

Bazargani, N., & Attwell, D. (2016). Astrocyte calcium signaling: The third wave. *Nature Neuroscience*, *19*, 182–189.

Bergman, T. J., Beehner, J. C., Painter, M. C., & Gustison, M. L. (2019). The speech-like properties of nonhuman primate vocalizations. *Animal Behaviour*, *151*, 229–237.

Berkiks, I., Garcia-Segura, L. M., Nassiri, A., Mesfioui, A., Ouichou, A., Boulbaroud, S., Bahbiti, Y., Lopez-Rodriguez, A. B., Hasnaoui, E., & El Hessni, A. (2019). The sex differences of the behavior response to early life immune stimulation: Microglia and astrocytes involvement. *Physiology and Behavior*, *199*, 386–394.

Bezzi, P., Carmignoto, G., Pasti, L., Vesce, S., Rossi, D., Rizzini, B. L., Pozzan, T., & Volterra, A. (1998). Prostaglandins stimulate calcium-dependent glutamate release in astrocytes. *Nature*, *391*, 281–285.

Bröer, S., Rahman, B., Pellegri, G., Pellerin, L., Martin, J. L., Verleysdonk, S., Hamprecht, B., & Magistretti, P. J. (1997). Comparison of lactate transport in astroglial cells and monocarboxylate transporter 1 (MCT 1) expressing *Xenopus laevis* oocytes. Expression of two different monocarboxylate transporters in astroglial cells and neurons. *Journal of Biological Chemistry*, *272*, 30096–30102.

Buosi, A. S., Matias, I., Araujo, A. P. B., Batista, C., & Gomes, F. C. A. (2018). Heterogeneity in synaptogenic profile of astrocytes from different brain regions. *Molecular Neurobiology*, *55*, 751–762.

Burman, K. J., Bakola, S., Richardson, K. E., Yu, H.-H., Reser, D. H., & Rosa, M. G. P. (2015). Cortical and thalamic projections to cytoarchitectural areas 6Va and 8C of the marmoset monkey: Connectionally distinct subdivisions of the lateral premotor cortex. *The Journal of Comparative Neurology*, *523*, 1222–1247.

Burman, K. J., Palmer, S. M., Gamberini, M., Spitzer, M. W., & Rosa, M. G. P. (2008). Anatomical and physiological definition of the motor cortex of the marmoset monkey. *The Journal of Comparative Neurology*, *506*, 860–876.

Bushong, E. A., Martone, M. E., Jones, Y. Z., & Ellisman, M. H. (2002). Protoplasmic astrocytes in CA1 stratum radiatum occupy separate anatomical domains. *The Journal of Neuroscience*, *22*, 183–192.

Cengiz, P., Zafer, D., Chandrashekhar, J. H., Chanana, V., Bogost, J., Waldman, A., Novak, B., Kintner, D. B., & Ferrazzano, P. A. (2019). Developmental differences in microglia morphology and gene expression during normal brain development and in response to hypoxia-ischemia. *Neurochemistry International*, *127*, 137–147.

Chai, H., Diaz-Castro, B., Shigetomi, E., Monte, E., Octeau, J. C., Yu, X., Cohn, W., Rajendran, P. S., Vondriska, T. M., Whitelegge, J. P., Coppola, G., & Khakh, B. S. (2017). Neural circuit-specialized astrocytes: Transcriptomic, proteomic, morphological, and functional evidence. *Neuron*, *95*, 531–549.e9.

Christensen, R. K., Petersen, A. V., & Perrier, J.-F. (2013). How do glial cells contribute to motor control? *Current Pharmaceutical Design*, *19*, 4385–4399.

Colombo, J. (2018). Interlaminar glia and other glial themes revisited: pending answers following three decades of glial research. *Neuroglia*, *1* (1), 7–20.

Colombo, J. A. (1996). Interlaminar astroglial processes in the cerebral cortex of adult monkeys but not of adult rats. *Acta Anatomica (Basel)*, *155*, 57–62.

Colombo, J. A. (2017). The interlaminar glia: From serendipity to hypothesis. *Brain Structure & Function*, *222*, 1109–1129.

Colombo, J. A., Fuchs, E., Härtig, W., Marotte, L. R., & Puissant, V. (2000). "Rodent-like" and "primate-like" types of astroglial architecture in the adult cerebral cortex of mammals: A comparative study. *Anatomy Embryology (Berlin)*, *201*, 111–120.

Colombo, J. A., & Reisin, H. D. (2004). Interlaminar astroglia of the cerebral cortex: A marker of the primate brain. *Brain Research*, *1006*, 126–131.

Costa, L. F. (1995). Computer vision based morphometric characterization of neural cells. *The Review of Scientific Instruments*, *66*, 3770–3773.

Covelo, A., & Araque, A. (2018). Neuronal activity determines distinct gliotransmitter release from a single astrocyte. *eLife*, *7*.

D'Ambrosio, R., Gordon, D. S., & Winn, H. R. (2002). Differential role of KIR channel and Na(+)/K(+)-pump in the regulation of extracellular K (+) in rat hippocampus. *Journal of Neurophysiology*, *87*, 87–102.

De Salles, A. A., Melega, W. P., Laćan, G., Steele, L. J., & Solberg, T. D. (2001). Radiosurgery performed with the aid of a 3-mm collimator in the subthalamic nucleus and substantia nigra of the vervet monkey. *Journal of Neurosurgery*, *95*, 990–997.

Debus, E., Weber, K. & Osborn, M. (1983). Monoclonal antibodies specific for glial fibrillary acidic (GFA) protein and for each of the neurofilament triplet polypeptides. *Differentiation; Research in Biological Diversity 25*(2), 193–203.

Dominy, S. S., Lynch, C., Ermini, F., Benedyk, M., Marczyk, A., Konradi, A., Nguyen, M., Haditsch, U., Raha, D., Griffin, C., Holsinger, L. J., Arastu-Kapur, S., Kaba, S., Lee, A., Ryder, M. I., Potempa, B., Mydel, P., Hellvard, A., Adamowicz, K., … Potempa, J. (2019). *Porphyromonas gingivalis* in Alzheimer's disease brains: Evidence for disease causation and treatment with small-molecule inhibitors. *Science Advances*, *5*, eaau3333.

Doyle, H. H., Eidson, L. N., Sinkiewicz, D. M., & Murphy, A. Z. (2017). Sex differences in microglia activity within the periaqueductal gray of the rat: A potential mechanism driving the dimorphic effects of morphine. *The Journal of Neuroscience*, *37*, 3202–3214.

Dringen, R., Gebhardt, R., & Hamprecht, B. (1993). Glycogen in astrocytes: Possible function as lactate supply for neighboring cells. *Brain Research*, *623*, 208–214.

Durkee, C., & Araque, A. (2019). Diversity and specificity of astrocyte–neuron communication. *Neuroscience*, *396*, 73–78.

Eilam, R., Aharoni, R., Arnon, R., & Malach, R. (2016). Astrocyte morphology is confined by cortical functional boundaries in mammals ranging from mice to human. *eLife*, 5.

Eliades, S. J., & Miller, C. T. (2017). Marmoset vocal communication: Behavior and neurobiology. *Developmental Neurobiology*, *77*, 286–299.

Eng, L. F. (1985). Glial fibrillary acidic protein (GFAP): The major protein of glial intermediate filaments in differentiated astrocytes. *Journal of Neuroimmunology*, *8*, 203–214.

Eng, L. F., Ghirnikar, R. S., & Lee, Y. L. (2000). Glial fibrillary acidic protein: GFAP-thirty-one years (1969-2000). *Neurochemical Research*, *25*, 1439–1451.

Falcone, C., Wolf-Ochoa, M., Amina, S., Hong, T., Vakilzadeh, G., Hopkins, W. D., Hof, P. R., Sherwood, C. C., Manger, P. R., Noctor, S. C., & Martínez-Cerdeño, V. (2019). Cortical interlaminar astrocytes across the therian mammal radiation. *The Journal of Comparative Neurology*, *527*, 1654–1674.

Forny-Germano, L., Lyra e Silva, N. M., Batista, A. F., Brito-Moreira, J., Gralle, M., Boehnke, S. E., Coe, B. C., Lablans, A., Marques, S. A., Martinez, A. M. B., Klein, W. L., Houzel, J-C., Ferreira, S. T., Munoz, D. P., & De Felice, F. G. (2014). Alzheimer's disease-like pathology induced by amyloid-β oligomers in nonhuman primates. *The Journal of Neuroscience*, *34*(41), 13629–13643.

Fuertinger, S., Zinn, J. C., Sharan, A. D., Hamzei-Sichani, F., & Simonyan, K. (2018). Dopamine drives left-hemispheric lateralization of neural networks during human speech. *The Journal of Comparative Neurology*, *526*, 920–931.

Ghazanfar, A. A., Liao, D. A., & Takahashi, D. Y. (2019). Volition and learning in primate vocal behaviour. *Animal Behaviour*, *151*, 239–247.

Ghazanfar, A. A., Takahashi, D. Y., Mathur, N., & Fitch, W. T. (2012). Cineradiography of monkey lip-smacking reveals putative precursors of speech dynamics. *Current Biology*, *22*, 1176–1182.

Gustison, M. L., Borjon, J. I., Takahashi, D. Y., & Ghazanfar, A. A. (2019). Vocal and locomotor coordination develops in association with the autonomic nervous system. *eLife*, *8*.

Halassa, M. M., Fellin, T., & Haydon, P. G. (2009). Tripartite synapses: Roles for astrocytic purines in the control of synaptic physiology and behavior. *Neuropharmacology*, *57*, 343–346.

Han, T.-U., Root, J., Reyes, L. D., Huchinson, E. B., du Hoffmann, J., Lee, W.-S., Barnes, T. D., & Drayna, D. (2019). Human GNPTAB stuttering mutations engineered into mice cause vocalization deficits and astrocyte pathology in the corpus callosum. *Proceedings of the National Academy of Sciences of the United States of America*, *116*, 17515–17524.

Harada, K., Kamiya, T., & Tsuboi, T. (2015). Gliotransmitter release from astrocytes: Functional, developmental, and pathological implications in the brain. *Frontiers in Neuroscience*, *9*, 499.

Haydon, P. G., & Carmignoto, G. (2006). Astrocyte control of synaptic transmission and neurovascular coupling. *Physiological Reviews*, *86*, 1009–1031.

Hefendehl, J. K., Neher, J. J., Sühs, R. B., Kohsaka, S., Skodras, A., & Jucker, M. (2014). Homeostatic and injury-induced microglia behavior in the aging brain. *Aging Cell*, *13*, 60–69.

Hegyi, Z., Kis, G., Holló, K., Ledent, C., & Antal, M. (2009). Neuronal and glial localization of the cannabinoid-1 receptor in the superficial spinal dorsal horn of the rodent spinal cord. *The European Journal of Neuroscience*, *30*, 251–262.

Hegyi, Z., Oláh, T., Kőszeghy, Á., Piscitelli, F., Holló, K., Pál, B., Csernoch, L., Di Marzo, V., & Antal, M. (2018). CB1 receptor activation induces intracellular Ca2+ mobilization and 2-arachidonoylglycerol release in rodent spinal cord astrocytes. *Scientific Reports*, *8*, 10562.

Heindl, S., Gesierich, B., Benakis, C., Llovera, G., Duering, M., & Liesz, A. (2018). Automated morphological analysis of microglia after stroke. *Frontiers in Cellular Neuroscience*, *12*, 106.

Himeda, T., Watanabe, Y., Tounai, H., Hayakawa, N., Kato, H., & Araki, T. (2006). Time dependent alterations of co-localization of S100beta and GFAP in the MPTP-treated mice. *Journal of Neural Transmission*, *113*, 1887–1894.

Jarvis, E.D. (2019). Evolution of vocal learning and spoken language. Science.

Jürgens, U. (2002). Neural pathways underlying vocal control. *Neuroscience and Biobehavioral Reviews*, *26*, 235–258.

Kang, Y., Ai, Z., Duan, K., Si, C., Wang, Y., Zheng, Y., He, J., Yin, Y., Zhao, S., Niu, B., Zhu, X., Liu, L., Xiang, L., Zhang, L., Niu, Y., Ji, W., & Li, T. (2018). Improving cell survival in injected embryos allows primed pluripotent stem cells to generate chimeric cynomolgus monkeys. *Cell Reports*, *25*, 2563–2576.e9.

Karperien, A., Ahammer, H., & Jelinek, H. F. (2013). Quantitating the subtleties of microglial morphology with fractal analysis. *Frontiers in Cellular Neuroscience*, *7*, 3.

Kasymov, V., Larina, O., Castaldo, C., Marina, N., Patrushev, M., Kasparov, S., & Gourine, A. V. (2013). Differential sensitivity of brainstem versus cortical astrocytes to changes in pH reveals functional regional specialization of astroglia. *The Journal of Neuroscience*, *33*, 435–441.

Kato, Y., Gokan, H., Oh-Nishi, A., Suhara, T., Watanabe, S., & Minamimoto, T. (2014). Vocalizations associated with anxiety and fear in the common marmoset (*Callithrix jacchus*). *Behavioural Brain Research*, *275*, 43–52.

Key, G., Petersen, J. L., Becker, M. H., Duchrow, M., Schlüter, C., Askaa, J., & Gerdes, J. (1993). New antiserum against Ki-67 antigen suitable for double immunostaining of paraffin wax sections. *Journal of Clinical Pathology*, *46*, 1080–1084.

Khakh, B. S., & Sofroniew, M. V. (2015). Diversity of astrocyte functions and phenotypes in neural circuits. *Nature Neuroscience*, *18*, 942–952.

Korogod, N., Petersen, C. C. H., & Knott, G. W. (2015). Ultrastructural analysis of adult mouse neocortex comparing aldehyde perfusion with cryo fixation. *eLife*, *4*.

Lehre, K. P., Levy, L. M., Ottersen, O. P., Storm-Mathisen, J., & Danbolt, N. C. (1995). Differential expression of two glial glutamate transporters in the rat brain: Quantitative and immunocytochemical observations. *The Journal of Neuroscience*, *15*, 1835–1853.

López-Hidalgo, M., & Schummers, J. (2014). Cortical maps: A role for astrocytes? *Current Opinion in Neurobiology*, *24*, 176–189.

Magistretti, P. J. (2006). Neuron-glia metabolic coupling and plasticity. *The Journal of Experimental Biology*, *209*, 2304–2311.

Maguire, G. A., Yoo, B. R., & SheikhBahaei, S. (2021). Investigation of risperidone treatment associated with enhanced brain activity in patients who stutter. *Frontiers in Neuroscience*, *15*, 598949.

Marina, N., Turovsky, E., Christie, I. N., Hosford, P. S., Hadjihambi, A., Korsak, A., Ang, R., Mastitskaya, S., Sheikhbahaei, S., Theparambil, S. M., & Gourine, A. V. (2018). Brain metabolic sensing and metabolic signaling at the level of an astrocyte. *Glia*, *66*, 1185–1199.

Miller, C. T., Freiwald, W. A., Leopold, D. A., Mitchell, J. F., Silva, A. C., & Wang, X. (2016). Marmosets: A neuroscientific model of human social behavior. *Neuron*, *90*, 219–233.

Miller, C. T., Thomas, A. W., Nummela, S. U., & de la Mothe, L. A. (2015). Responses of primate frontal cortex neurons during natural vocal communication. *Journal of Neurophysiology*, *114*, 1158–1171.

Mishra, A., Reynolds, J. P., Chen, Y., Gourine, A. V., Rusakov, D. A., & Attwell, D. (2016). Astrocytes mediate neurovascular signaling to capillary pericytes but not to arterioles. *Nature Neuroscience*, *19*, 1619–1627.

Mong, J. A., & McCarthy, M. M. (2002). Ontogeny of sexually dimorphic astrocytes in the neonatal rat arcuate. *Brain Research. Developmental Brain Research*, *139*, 151–158.

Morquette, P., Verdier, D., Kadala, A., Féthière, J., Philippe, A. G., Robitaille, R., & Kolta, A. (2015). An astrocyte-dependent mechanism for neuronal rhythmogenesis. *Nature Neuroscience*, *18*, 844–854.

Morrill, R. J., Paukner, A., Ferrari, P. F., & Ghazanfar, A. A. (2012). Monkey lipsmacking develops like the human speech rhythm. *Developmental Science*, *15*, 557–568.

Moye, S. L., Diaz-Castro, B., Gangwani, M. R., & Khakh, B. S. (2019). Visualizing astrocyte morphology using lucifer yellow Iontophoresis. *Journal of Visualized Experiments*, *151*.

Oberheim Bush, N. A., & Nedergaard, M. (2017). Do evolutionary changes in astrocytes contribute to the computational power of the hominid brain? *Neurochemical Research*, *42*, 2577–2587.

Oberheim, N. A., Goldman, S. A., & Nedergaard, M. (2012). Heterogeneity of astrocytic form and function. *Methods in Molecular Biology*, *814*, 23–45.

Oberheim, N. A., Takano, T., Han, X., He, W., Lin, J. H. C., Wang, F., Xu, Q., Wyatt, J. D., Pilcher, W., Ojemann, J. G., Ransom, B. R., Goldman, S. A., & Nedergaard, M. (2009). Uniquely hominid features of adult human astrocytes. *The Journal of Neuroscience*, *29*, 3276–3287.

Oberheim, N. A., Tian, G.-F., Han, X., Peng, W., Takano, T., Ransom, B., & Nedergaard, M. (2008). Loss of astrocytic domain organization in the epileptic brain. *The Journal of Neuroscience*, *28*, 3264–3276.

Oberheim, N. A., Wang, X., Goldman, S., & Nedergaard, M. (2006). Astrocytic complexity distinguishes the human brain. *Trends in Neurosciences*, *29*, 547–553.

Okano, H., Hikishima, K., Iriki, A., & Sasaki, E. (2012). The common marmoset as a novel animal model system for biomedical and neuroscience research applications. *Seminars in Fetal & Neonatal Medicine*, *17*, 336–340.

Oliveira, J. F., Sardinha, V. M., Guerra-Gomes, S., Araque, A., & Sousa, N. (2015). Do stars govern our actions? Astrocyte involvement in rodent behavior. *Trends in Neurosciences*, *38*, 535–549.

Parpura, V., & Haydon, P. G. (2000). Physiological astrocytic calcium levels stimulate glutamate release to modulate adjacent neurons. *Proceedings of the National Academy of Sciences of the United States of America*, *97*, 8629–8634.

Paxinos, G., Watson, C., Petrides, M., Rosa, M., Tokuno, H. (2012). The marmoset brain in stereotaxic coordinates.

Pellerin, L., Pellegri, G., Bittar, P. G., Charnay, Y., Bouras, C., Martin, J. L., Stella, N., & Magistretti, P. J. (1998). Evidence supporting the existence of an activity-dependent astrocyte-neuron lactate shuttle. *Developmental Neuroscience*, *20*, 291–299.

Petrides, M., Cadoret, G., & Mackey, S. (2005). Orofacial somatomotor responses in the macaque monkey homologue of Broca's area. *Nature*, *435*, 1235–1238.

Pomberger, T., Risueno-Segovia, C., Gultekin, Y. B., Dohmen, D., & Hage, S. R. (2019). Cognitive control of complex motor behavior in marmoset monkeys. *Nature Communications*, *10*(1), 3796.

Power, R. A., Power, M. L., Layne, D. G., Jaquish, C. E., Oftedal, O. T., & Tardif, S. D. (2001). Relations among measures of body composition, age, and sex in the common marmoset monkey (*Callithrix jacchus*). *Comparative Medicine*, *51*, 218–223.

Radford, R., Rcom-H'cheo-Gauthier, A., Wong, M. B., Eaton, E. D., Quilty, M., Blizzard, C., Norazit, A., Meedeniya, A., Vickers, J. C., Gai, W. P., Guillemin, G. J., West, A. K., Dickson, T. C., Chung, R., & Pountney, D. L. (2015). The degree of astrocyte activation in multiple system atrophy is inversely proportional to the distance to α-synuclein inclusions. *Molecular and Cellular Neurosciences*, *65*, 68–81.

Rajani, V., Zhang, Y., Jalubula, V., Rancic, V., SheikhBahaei, S., Zwicker, J. D., Pagliardini, S., Dickson, C. T., Ballanyi, K., Kasparov, S., Gourine, A. V., & Funk, G. D. (2018). Release of ATP by pre-Bötzinger complex astrocytes contributes to the hypoxic ventilatory response via a Ca^{2+} −dependent $P2Y_1$ receptor mechanism. *The Journal of Physiology*, *596*, 3245–3269.

Reeves, A. M. B., Shigetomi, E., & Khakh, B. S. (2011). Bulk loading of calcium indicator dyes to study astrocyte physiology: Key limitations and improvements using morphological maps. *The Journal of Neuroscience*, *31*, 9353–9358.

Sadagopan, S., Temiz-Karayol, N. Z., & Voss, H. U. (2015). High-field functional magnetic resonance imaging of vocalization processing in marmosets. *Scientific Reports*, *5*, 10950.

Santello, M., Toni, N., & Volterra, A. (2019). Astrocyte function from information processing to cognition and cognitive impairment. *Nature Neuroscience*, *22*, 154–166.

Sheikhbahaei, S., Morris, B., Collina, J., Anjum, S., Znati, S., Gamarra, J., Zhang, R., Gourine, A. V., & Smith, J. C. (2018). Morphometric analysis of astrocytes in brainstem respiratory regions. *The Journal of Comparative Neurology*, *526*, 2032–2047.

Sheikhbahaei, S., Turovsky, E. A., Hosford, P. S., Hadjihambi, A., Theparambil, S. M., Liu, B., Marina, N., Teschemacher, A. G., Kasparov, S., Smith, J. C., & Gourine, A. V. (2018). Astrocytes modulate brainstem respiratory rhythm-generating circuits and determine exercise capacity. *Nature Communications*, *9*, 370.

Sholl, D. A. (1953). Dendritic organization in the neurons of the visual and motor cortices of the cat. *Journal of Anatomy*, *87*, 387–406.

Simard, M., & Nedergaard, M. (2004). The neurobiology of glia in the context of water and ion homeostasis. *Neuroscience*, *129*, 877–896.

Simões, C. S., Vianney, P. V. R., de Moura, M. M., Freire, M. A. M., Mello, L. E., Sameshima, K., Araújo, J. F., Nicolelis, M. A. L., Mello, C. V., & Ribeiro, S. (2010). Activation of frontal neocortical areas by vocal production in marmosets. *Frontiers in Integrative Neuroscience*, *4*.

Simonyan, K., & Fuertinger, S. (2015). Speech networks at rest and in action: Interactions between functional brain networks controlling speech production. *Journal of Neurophysiology*, *113*, 2967–2978.

Smith, C. J., & Bilbo, S. D. (2019). Microglia sculpt sex differences in social behavior. *Neuron*, *102*, 275–277.

Tavares, G., Martins, M., Correia, J. S., Sardinha, V. M., Guerra-Gomes, S., das Neves, S. P., Marques, F., Sousa, N., Oliveira, J. F. (2017). Employing an open-source tool to assess astrocyte tridimensional structure. *Brain Structure and Function*, *222*(4), 1989–1999.

Theodoni, P., Majka, P., Reser, D. H., Wójcik, D. K., Rosa, M. G. P., & Wang, X-J. (2021). Structural attributes and principles of the neocortical connectome in the marmoset monkey. *Cerebral Cortex*, bhab191.

Thiruvalluvan, A., Czepiel, M., Kap, Y. A., Mantingh-Otter, I., Vainchtein, I., Kuipers, J., Bijlard, M., Baron, W., Giepmans, B., Brück, W., 't Hart, B. A., Boddeke, E., & Copray, S. (2016). Survival and functionality of human induced pluripotent stem cell-derived oligodendrocytes in a nonhuman primate model for multiple sclerosis. *STEM CELLS Translational Medicine*, *5*(11), 1550–1561.

Turk, A. Z., Lotfi Marchoubeh, M., Fritsch, I., Maguire, G. A., & SheikhBahaei, S. (2021). Dopamine, vocalization, and astrocytes. *Brain and Language*, *219*, 104970.

Ventura, R., & Harris, K. M. (1999). Three-dimensional relationships between hippocampal synapses and astrocytes. *The Journal of Neuroscience*, *19*, 6897–6906.

Verkhratsky, A., Bush, N., Nedergaard, M., & Butt, A. (2018). The special case of human astrocytes. *Neuroglia*, *1*(1), 21–29.

Vigneau, M., Beaucousin, V., Hervé, P. Y., Duffau, H., Crivello, F., Houdé, O., Mazoyer, B., & Tzourio-Mazoyer, N. (2006). Meta-analyzing left hemisphere language areas: Phonology, semantics, and sentence processing. *NeuroImage*, *30*, 1414–1432.

Volterra, A., & Meldolesi, J. (2005). Astrocytes, from brain glue to communication elements: The revolution continues. *Nature Reviews. Neuroscience*, *6*, 626–640.

Wagner, B., Natarajan, A., Grünaug, S., Kroismayr, R., Wagner, E. F., & Sibilia, M. (2006). Neuronal survival depends on EGFR signaling in cortical but not midbrain astrocytes. *The EMBO Journal*, *25*, 752–762.

Wagner, D.-C., Scheibe, J., Glocke, I., Weise, G., Deten, A., Boltze, J., & Kranz, A. (2013). Object-based analysis of astroglial reaction and astrocyte subtype morphology after ischemic brain injury. *Acta Neurobiologiae Experimentalis (Wars)*, *73*, 79–87.

Walz, W. (1989). Role of glial cells in the regulation of the brain ion microenvironment. *Progress in Neurobiology*, *33*, 309–333.

Wu, X., Liu, Y., Chen, X., Sun, Q., Tang, R., Wang, W., Yu, Z., & Xie, M. (2013). Involvement of TREK-1 activity in astrocyte function and neuroprotection under simulated ischemia conditions. *Journal of Molecular Neuroscience*, *49*, 499–506.

Xin, W., Schuebel, K. E., Jair, K.-W., Cimbro, R., De Biase, L. M., Goldman, D., & Bonci, A. (2019). Ventral midbrain astrocytes display unique physiological features and sensitivity to dopamine D2 receptor signaling. *Neuropsychopharmacology*, *44*, 344–355.

Xu, H., Gelyana, E., Rajsombath, M., Yang, T., Li, S., & Selkoe, D. (2016). Environmental enrichment potently prevents microglia-mediated neuroinflammation by human amyloid -protein oligomers. *Journal of Neuroscience*, *36*(35), 9041–9056.

Yu, X., Nagai, J., & Khakh, B. S. (2020). Improved tools to study astrocytes. *Nature Reviews Neuroscience*, *21*(3), 121–138.

Zhou, B., Chen, L., Liao, P., Huang, L., Chen, Z., Liao, D., Yang, L., Wang, J., Yu, G., Wang, L., Zhang, J., Zuo, Y., Liu, J., & Jiang, R. (2019). Astroglial dysfunctions drive aberrant synaptogenesis and social behavioral deficits in mice with neonatal exposure to lengthy general anesthesia. *PLoS Biology*, *17*, e3000086.

Zilles, K., Armstrong, E., Moser, K. H., Schleicher, A., & Stephan, H. (1989). Gyrification in the cerebral cortex of primates. *Brain, Behavior and Evolution*, *34*, 143–150.

SUPPORTING INFORMATION

Additional supporting information may be found in the online version of the article at the publisher's website.

How to cite this article: Turk, A. Z., & SheikhBahaei, S. (2022). Morphometric analysis of astrocytes in vocal production circuits of common marmoset (*Callithrix jacchus*). *Journal of Comparative Neurology*, *530*(2), 574–589. https://doi.org/10.1002/cne.25230